

# Heat Loss Evaluation of an Experimental Set-up for predicting the Initial Stage of the Boiling Curve for Water at Low Pressure

K. T. Witte<sup>\*1</sup>, F. Dammel<sup>2</sup>, L. Schnabel<sup>1</sup> and P. Stephan<sup>2</sup>

<sup>1</sup>Fraunhofer Institut Solare Energiesysteme, <sup>2</sup>Technische Universität Darmstadt

\* Heidenhofstraße 2, 79110 Freiburg, kai.witte@ise.fraunhofer.de

**Abstract:** In this paper heat losses and gains are assessed for a specific measuring set-up in order to improve the validity of performance data to accurately predict the initial stage of a boiling curve, using water as refrigerant. Simulation focus on achieving results predicting real measuring data of a plain surface structure at a saturation temperature of 7,24 ° C. Therefore, the relevant components of the measuring set-up have been implemented in a 2-D axisymmetric model combining the Physics 'Heat Transfer in Fluids - laminar flow' with 'Heat Transfer in Solids'. The heat transfer by conduction and radiation has been combined as well as each relevant data were obtained from VDI-Heat Atlas. The operability of the model has been proven analyzing the simulation results and the influence of heat losses and gains are investigated by varying model parameters. Thus, the influence on the boiling curve of a plain copper surface as well as for a metallic short fiber structure has been roughly estimated. Finally, the measured results of the plain surface structure and one adapted simulation result are compared to a correlation.

**Keywords:** Free Convection, Laminar Flow, Buoyancy Flow, Heat Transfer Coefficient, Boiling Curve.

## 1. Introduction

Even though there is extensive literature on evaporation of water, data on the evaporation at low pressure conditions – as they are required to design evaporators for ab- and adsorption chillers - are still scarce, especially to predict the heat transfer coefficients during nucleate boiling. Thus, the correlation from Gorenflo and Kenning [1] is recommended for a lower pressure limit of 100 mbar while he explicitly points out that nucleation at even lower pressures differs drastically from that at higher pressures. Stephan [2] attributes the reason for a lack of a coherent theory to the complex interactions of the various heat and mass transport processes and on the various characteristic length scales involved in boiling

heat transfer. Observing the potential of different surface structures to design evaporators requires the knowledge of its boiling curve. These curves are typically generated in order to determine the heat transfer coefficient  $\alpha$  at pool boiling as it is required for evaporator dimensioning (two phase heat transfer). They describe the correlation between heat flux density (W/m<sup>2</sup>) and wall superheat (K) - defined as difference between wall temperature and saturation temperature - and include the knowledge of the boiling regime [3].

In order to investigate the initial stage of the boiling curve, i.e. convective and nucleate boiling, for different kinds of surface structures a measuring rig has been set into operation at Fraunhofer ISE. Thereby it was especially focused on realizing very low filling levels of the water in order to analyze capillary-assisted wetting of metallic short fiber structures – not only entirely flooded. As the measuring set-up itself has an impact on the accuracy in predicting the characteristic values of the boiling curve, this contribution focuses on detecting and evaluating these measuring uncertainties in order to finally present accurate boiling curves.

For this reason the measuring set-up is presented first showing the influencing factors as well as measuring data provided to evaluate the simulation finally. The mathematical explanation of the problem and the implementation to COMSOL Version 4.2 follows before the simulation results are presented and their influence on the measuring results is discussed.

## 2. Experimental set-up and used measuring data

Figure 1 shows a scheme of the measuring set-up to determine the pool boiling curves. The evaporation takes place inside the vacuum chamber (3) which is pictured more detailed via the cross-sectional view in Figure 2. Here, different kinds of samples (e.g. smoothed or surfaces with a metallic short fiber structure) are mounted horizontally on a heater. The

water is supplied below the ‘real’ sample through an exterior PMMA tube (acrylic glass) where it is re-filled through a by-pass channel that allows to set different filling levels using the ‘U-tube-effect’.

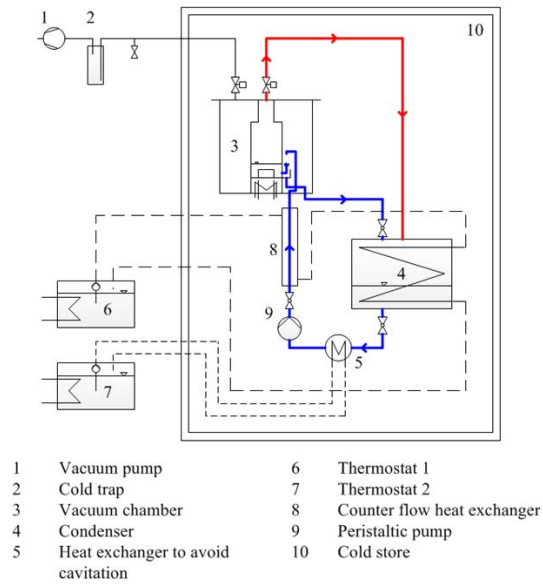


**Figure 1.** Hydraulic scheme of the measuring set-up.

Thus, theoretically each filling level - depending on the surface wettability - can be adjusted. The dark blue lines indicate the liquid part of the refrigerant (water supply to the sample as well as the rejection of excessive water) and the red line shows the path of the steam from the evaporator (3) to the condenser (4).

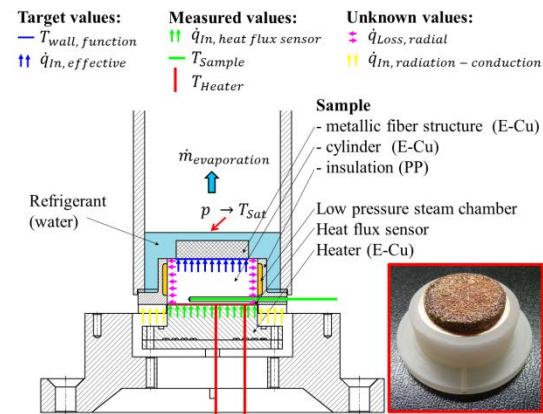


**Figure 2.** Experimental set-up to demonstrate the boiling pool with relevant components, energy flows and temperature measurement as well as a cut-out of a metallic short fiber sample (bottom right corner).

The main components are built up inside a cold store in order to reduce heat input from the ambient. Thus, the required ambient temperature is set according to the International Steam Tables by Wagner and Kretschmar [4]. E.g. the determination of a boiling curve at 10 mbar requires an ambient temperature of approximately 7 °C. To create a boiling curve the heat flux (cf. in Figure 2) is measured as a function of the wall superheat evaluated after reaching stationary conditions (cf. ‘Analysis area’ in Figure 3). Therefore, pre-defined electrical power steps are set after each other to the heater leading to an increase in heat flux (cf. ‘\_Heater’ and ‘Heat flux’ in Figure 3).

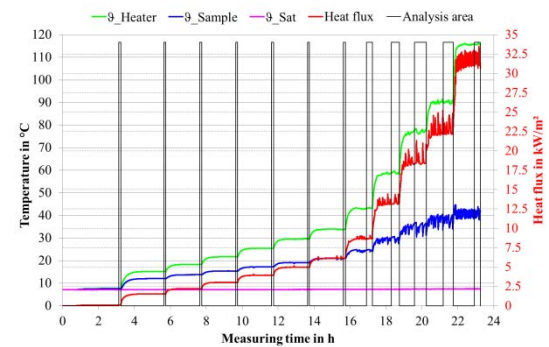


**Figure 3.** Measuring data of the plain surface structure serving as model's input as well as for validation purposes.

Moreover, Figure 3 shows the measuring data serving for the model as input values, i.e. ‘\_Heater’, ‘\_Sat’ and the ‘Heat flux’ (also refer to Figure 2) as well as the useful output ‘\_Sample’ to validate the simulation results finally. Annotation: The initiation of bubble formation during the measurements occurred much earlier as expected, i.e. already at wall superheats of approx. 14 K, in comparison to earlier studies by Schnabel et al. [5] where the initiation of nucleate boiling could be observed at wall superheats of approx. 25 K for a different kind of measuring set-up. This behavior has been expected and is addressed to the set-up of the sample. Thus, bubble formation starts at the contact area between the copper cylinder and the PP-insulation as nucleation sites are trapped here very easily and additionally a local hot spot promotes the bubble initiation. Even though the results for plain surfaces are falsified within the single bubble region for this kind of sample set-up, this influence is expected to be negligible for

the actual samples of interest - i.e. the metallic short fiber structures (cf. cutout in Figure 2). Here, the initiation of nucleate boiling could have been observed at wall superheats of already approx. 10 K (cf. Figure 10). Each temperature sensor has been calibrated. Thus, an extended uncertainty ( ) of approx.

has been evaluated. Taking a temperature decrease especially from the sample temperature measurement into account an uncertainty of less than is expected. The extended uncertainty of the measured heat flux is presented in Table 1 while the influence of the data logger gets visible observing the trend to very little heat fluxes.

**Table 1:** Extended uncertainty for varying measured heat fluxes

Measured heat flux W/m <sup>2</sup>	Extended uncertainty (k = 2) %
1	726.84
100	9.29
200	6.83
500	5.96
1000	5.82
10000	5.77
20000	5.77

### 3. Comsol Implementation with boundary conditions

Figure 4 shows the implementation of the problem into COMSOL through a 2-D axisymmetric model while symbols, units (SI units) and dimensionless numbers of the following equations are used according to the VDI Heat Atlas as presented in Table 1 of the appendix.

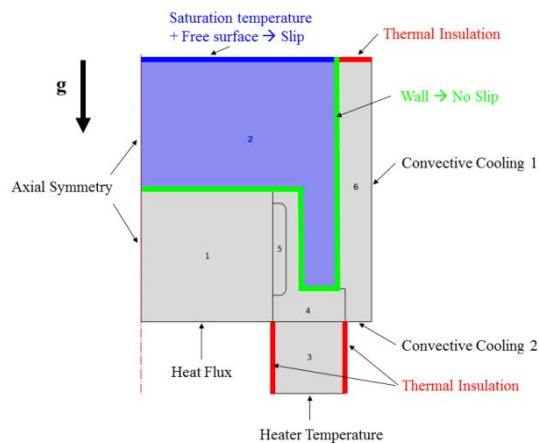


**Figure 4.** COMSOL Implementation with boundary conditions.

The blue highlighted area (2) in Figure 4 is represented through 'Heat Transfer in Fluids' applying 'laminar flow' (for an incompressible flow) according to the corresponding Rayleigh numbers of the regarded temperature differences, i.e. Ra or GrPr respectively are smaller than 70000 [1]. The laminar flow and the heat transfer interfaces in this area are 2-way coupled as reported in [6]. Therefore, a Boussinesq term (also body force) which accounts for the lifting force due to thermal expansion is added contrary to gravity direction (positive z-coordinate) to the right hand side of the incompressible Navier-Stokes equation:

$$(1)$$

$$(2)$$

enabling the fluid velocity to transport heat, while the fluid properties for the density  $\rho$  and the isobaric cubic expansion coefficient  $\beta$  of water were chosen from [4] for the corresponding local reference temperatures inside the pool - as reported in [7] at saturated liquid state. Thereby the wall temperatures were obtained by a first simulation cycle applying  $\beta$  at the saturation temperature of 7.24 °C. The heat balance comes from the conduction-convection equation:

$$(3)$$

For the fluid water is applied as available in COMSOL's data base, i.e. all properties depend on local temperature only. At the solid walls (cf. green lines in Figure 4) the boundary condition 'No Slip' is used while for the free water surface (cf. blue line in Figure 4) 'Slip' has been applied. The other areas are implemented through the 'Physics - Heat Transfer in Solids' which is represented through the steady-state heat equation with the volumetric heat source set to zero:

$$(4)$$

Here, material properties for the areas 1 (copper) and 6 (PMMA) could have been obtained directly from COMSOL's material browser while area 4 (PP) had to be created. The low pressure steam chamber (area 5) and the space between the heater and the insulation of the sample (area 3) were treated separately according to [8]. Thus, the low pressure steam chamber is considered as 'vertical rectilinear

enclosure' (Vertical Annuli) while the space between heater and the insulation of the sample (area 3) is treated as 'horizontal rectilinear enclosure' (Plane Horizontal Layer') – 'highly' approximated. The total heat flow rate within these enclosures is given by

$\dot{Q} = \frac{\lambda_{CCR} A}{L(T_1 - T_2)}$ , where  $\lambda_{CCR} = \lambda_R + \lambda_{CC}$  is the total thermal conductivity equivalent and in  $\lambda_R = 4sC_{12}T_m^3$  the thermal conductivity equivalent for radiation and  $\lambda_{CC} = Nu_s \lambda$  the thermal conductivity equivalent for convection and conduction [8]. Since the condition to reach a critical Rayleigh number ( $Ra_{crit}$ ), i.e.  $Ra > Ra_{crit}$  with  $Ra_{crit} = 1707.7$  for two solid isothermal walls [9] - as necessary condition for the formation of a convection current - has been far from being fulfilled ( $Ra_{max} = 1.4$ ) only heat conduction occurs inside both gaps. Thus,  $Nu_s$  turns to 1, i.e.  $\lambda_{CC} = \lambda$ . The determination of  $\lambda$  has been carried out at the corresponding reference temperatures  $T_{*,2} = T_m = \frac{1}{2}(T_1 + T_2)$ , where  $T_1$  was chosen as sample temperature and the heater temperature respectively and  $T_2$  as saturation temperature  $T_{Sat}$  and sample temperature respectively as first approximation. The radiation exchange number between the heater and the insulation of the sample (cf. area 3) is calculated following [10] via

$C_{12} = C_{H \rightarrow PP} = \frac{\sigma}{\frac{1}{\epsilon_H} + \frac{1}{\epsilon_{PP}} - 1}$  and for the low pressure steam chamber through

$C_{12} = C_{Cu,cyl \rightarrow PP} = \frac{\sigma}{\frac{1}{\epsilon_{Cu,cyl}} + \frac{A_{Cu,cyl}}{A_{PP}} \left( \frac{1}{\epsilon_{PP}} - 1 \right)}$ . Here,

Stefan-Boltzmann's constant  $\sigma = 5.67040 \times 10^{-8} \frac{W}{m^2 K^4}$  and emissivities of  $\epsilon_H = 0.3$ ,  $\epsilon_{PP} = 0.95$  and  $\epsilon_{Cu,cyl} = 0.5$  were applied according to the suggestions in [10] and [11] taking the surface treatment and shape into account. Finally, the determined total thermal conductivity equivalent  $\lambda_{CCR}$  for each case has been inserted as material data in area 5 and 3 respectively.

The assumed boundary conditions alongside the system boundary are also indicated in Figure 4. Here, the saturation temperature  $\vartheta_{Sat}$  has been applied as constant at 7.24 °C and its corresponding fluid ('steam') properties were used while determining the heat transfer coefficients  $\alpha$  for the boundaries at the peripheral surface ('Convective Cooling 1') and the lower front face of the PMMA-tube ('Convective Cooling 2'). In doing so, the

corresponding heat transfer coefficients were determined by  $\alpha = \frac{Nu \lambda}{L}$  while computing the Nusselt number for the peripheral surface (cf. VDI 'Vertical Surfaces' [7]) through

$$Nu = Nu_{plate} + 0.97 \frac{h}{D}$$

with the Nusselt number for a vertical plate

$$Nu_{(plate)} = \{0.825 + 0.387[Raf_1(Pr)]^{1/6}\}^2$$

and the height of the PMMA-tube as characteristic length L. For the lower front face the Nusselt number is computed via the suggestion for 'Heat Emission at Lower Surface (Upper Surface Cooled)' [7]

$$Nu = 0.6[Raf_1(Pr)]^{1/5}$$

and the characteristic length L for a circular

ring, i.e.  $L = \frac{(D^2 - d^2)}{4 \times (\frac{D-d}{2} + d)}$ . In both cases the

Rayleigh number is calculated via

$Ra = \frac{gL^3 \beta (T_s - T_\infty)}{\nu k}$  applying  $T_{Sat}$  as  $T_\infty$  and  $T_s$  as estimated surface temperature. The function  $f_1(Pr)$  is determined through

$$f_1(Pr) = \left[ 1 + \left( \frac{0.492}{Pr} \right)^{9/16} \right]^{-16/9}$$

Material properties are treated temperature-independent here while the values at saturation temperature  $T_{Sat} = T_\infty$  - that correspond to the average value of the entire measuring time (cf. Figure 3) - have been applied in a first step. In addition, a temperature gradient of 3 K has been estimated therefore. The values were evaluated at the local reference temperature  $T_{*,3} = \frac{1}{2}(T_s - T_\infty)$ .

A 'Normal - Free Triangular' mesh has been set up and especially a 'Boundary Layer' mesh for area 2 as it is typically used for fluid flow problems. To solve the problem the PARDISO solver (Direct Fully Coupled Stationary Solver) has been applied leading to a solution in each case at lower than 100 iterations.

## 4. Results

### 4.1 Validation of the COMSOL model

The validity of the COMSOL model is proven by both observing a provided temperature plot and by comparing the measuring data of the plain surface structure to the simulation results. Analyzing Figure 5 for the simulation result 8 - corresponding to a heat flux input of 6110 W/m<sup>2</sup> (cf. 'COMSOL\_P8' in Figure 6), a saturation temperature of 7.24 °C and a heater temperature of 33.82 °C - feasible results are obtained as the temperature inputs to the model are recognized, e.g. the lowest temperature corresponds to the saturation

temperature, and the temperature decrease from the sample cylinder as well as from the heater to the adjacent areas looks trustful. Furthermore, a vortex exists (cf. the red arrows) showing the operability of the buoyancy-driven convection.

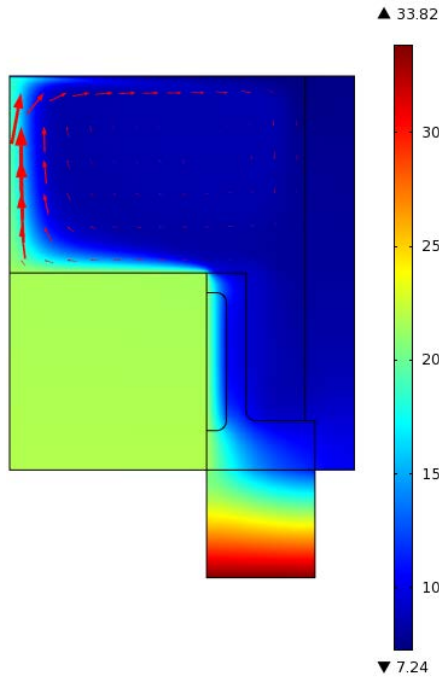


**Figure 5.** 2-D Plot Group for the temperature in °C and the velocity field (cf. red arrows) at simulation result 8.

In Figure 6 the measured temperatures in the sample are opposed to the simulated results including error bars with deviations from to - covering each compared value - in order to estimate the deviations.

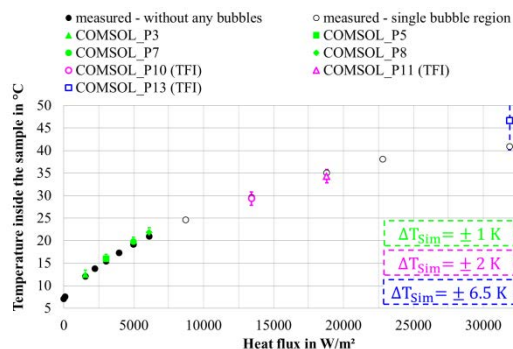


**Figure 6.** Measuring data versus simulation results as a function of the measured and inserted heat flux to the model.

The estimated extended measuring uncertainties of the temperature measurement inside the sample are not included as they are too small and would not have been noticed anyway. The measured values are further separated into results without any bubble formation during the measurements and into those where single bubbles occurred. This is obtained while analyzing the heat flux signal in Figure 3 concerning a scatter which shows the appearance of bubbles or not and is important to know as the initialization of bubbles significantly influences the heat transfer. Annotation: The Simulation results for the single bubble region could have been obtained only using a turbulent flow interface (TFI). Therefore the turbulent flow option has been selected applying the standard ‘Turbulence Model Parameters’. The corresponding theory is not discussed in this study as the experimental data for the region without any bubble formation are more meaningful (cf. Annotation in ‘2.’).

Analyzing the results, a good agreement between simulation and measured values is to observe. The measured values are only slightly overestimated, i.e., in the region without any bubble formation but also the initial values in the single bubble region are determined quite well with deviations of . The apparent deviation of the simulation result ‘COMSOL\_P13 (TFI)’ is addressed to the fact that the already well pronounced bubble initialization causes a better cooling of the sample, i.e. the heat transfer coefficient increases, as it is well known from literature (e.g. [1] and [3]) and presented within the general boiling curve behavior through a steeper slope of the axis. Here, the model assumption is simply wrong for this case and simulation of nucleate boiling is not possible with our COMSOL model. Nevertheless, also this result is applied to estimate the heat input from the heater to the sample as it will be shown in Figure 8.

Looking for adaptation options concerning the overestimated region without any bubble formation a rough sensitivity analysis is carried out based on the simulation result ‘COMSOL\_P8’ – corresponding to a heat flux input of 6100 W/m² (cf. Figure 6), a saturation temperature of 7.24 °C and a heater temperature of 33.82 °C. Thereby each influencing parameter has been increased or

decreased respectively by 6 % - according to the measuring uncertainty of the heat flux sensor (cf. Table 1) - with respect to the previously assumed values.

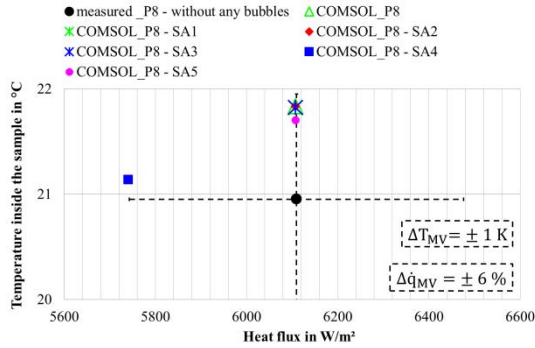


**Figure 7.** Measuring data versus simulation results as a function of the measured and inserted heat flux to the model for several simulation assumptions.

Figure 7 shows the obtained results. Thus, there is neither a recognizable influence to the sample temperature, decreasing the heat input from the heater stump to the sample concerning the Celsius temperature ('COMSOL\_P8 – SA1') nor by increasing the heat losses from the PMMA to the environment - by increasing the outer heat transfer coefficients  $\alpha$  (cf. 'COMSOL\_P8 – SA2' and 'Convective Cooling 1 + 2' in Figure 4) - or through increasing the total thermal conductivity equivalent inside the low pressure steam chamber ('COMSOL\_P8 – SA3'). In contrast to this, the increased isobaric thermal expansion coefficient reduces the sample temperature by approx. 0.1 K and the most significant influence on the temperature is caused by the decreased heat flux ('COMSOL\_P8 – SA4') while the change in heat input to the model is to take into account. Thus, the adaption of the model will primarily focus on the actual isobaric thermal expansion coefficient as outcome from further iterations. Additionally, the space between heater and the insulation of the sample (area 3 in Figure 4) - treated as 'horizontal rectilinear enclosure' (Plane Horizontal Layer) here – and its influence to the temperature inside the sample will be analyzed more carefully in further studies according to this contribution. The investigations in this study which are presented in following are based on the results of Figure 6.

## 4.2 Influence of the heat losses and gains at the plain surface structure

Adapted from the simulation results in Figure 6 the radial heat flow losses and gains as a function of the sample's temperature are presented in Figure 8. Additionally, one simulation result showing the radial heat flow losses without heat flow gains from the heater stump to the sample insulation (cf. red dot in Figure 8) is included. Due to this, the influence of the heat flow gains to the heat flow arriving on top of the surface is negligible under these simulation assumptions. In general, the heat losses and gains show a linear function suiting to the assumed linear heat conduction losses.

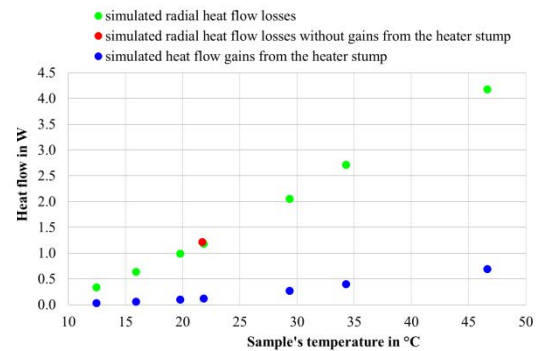


**Figure 8.** Radial heat flow losses and gains versus sample's temperature.

Figure 9 shows the influence of these values plotting the boiling curve for the plain surface structure both for the simulation results as well as for the measured values.

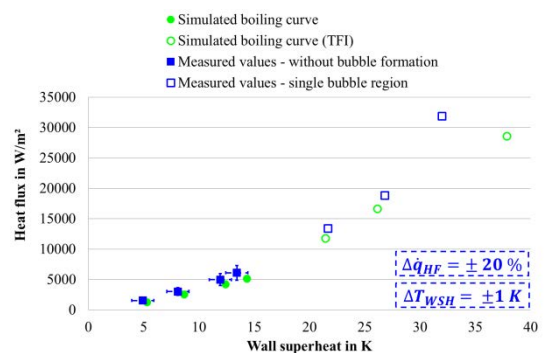


**Figure 9.** Influence of heat losses while analyzing the boiling curve for the plain surface structure – comparison of simulation to measuring results.

Focusing on the region without any bubble formation only, significant deviations are recognized. Thus, the radial heat losses of the sample cause a decrease of approx. 20 % for

the actual heat flux arriving on top of the surface (cf. in Figure 2). Furthermore, the wall superheat is nearly 1 K higher at the fourth simulation result as it is calculated for the measuring data - applying Fourier's law only, i.e. without taking any temperature decrease due to radial heat losses (cf. in Figure 2) into account. As a result of this, the necessity for rectifying the measuring data becomes obvious.

### 4.3 Estimation of the influence of the heat losses and gains to the boiling curve of the metallic short fiber structure

Measurements of the metallic short fiber structure in Figure 10 show that sample temperatures of maximum 20 °C during nucleate boiling occur.

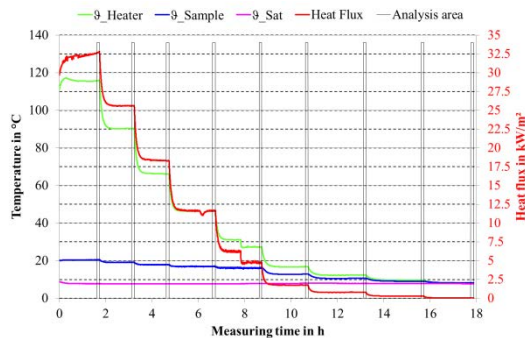


Figure 10. Measuring data of the metallic short fiber structure.

To estimate the influence of the heat losses and gains to the boiling curve of this structure the following steps were carried out. First, a simulation result for the plain surface structure close to this sample temperature has been selected. This was nearly fulfilled for 'COMSOL\_P7' (cf. Figure 6) with a sample temperature of 19.8 °C. After this, the heater temperature was changed according to Figure 10 to a value of 115 °C as well as the corresponding total thermal conductivity equivalent as described in '3.'. As a result, heat flow gains from the heater stump to the sample insulation of 0.73 W were obtained that are approximately seven times larger than those of the 'normal' plain surface structure, i.e. 0.10 W. Nevertheless, the influence of these gains to the radial heat flow losses is significantly lower. Thus, radial heat flow losses of 0.81 W were found in comparison to 0.99 W for the 'normal' simulation of the plain surface structure. Subtracting these losses from

the heat flow input of the experimental data of the metallic short fiber structure, i.e. from a value of 40.84 W which corresponds to 32500 W/m<sup>2</sup>, turns out in a decrease of the actual heat flux arriving on top of the surface (cf.

in Figure 2) of approx. 2 %. For this reason the influence of the radial heat losses seem to be negligible for this assumption as it is the same for the increase in wall temperature with a value of 0.03 K due to the reduced heat flow. Thereby the individual wall temperatures were calculated according to Fourier's law — in both

cases. Nevertheless, care has to be taken at lower heat fluxes as it is the case for the plain surface structure where these radial heat losses have a more pronounced impact. Concerning the metallic short fiber structure it is further to prove how the turbulent flow (nucleate boiling) in the upper part of the pool influences the heat transfer at the upper circular ring of the sample insulation but also the heat transfer at the lower pool part at the outer surface of the sample insulation (between PP and PMMA, cf. Figure 2, 4 and 5).

### 4.4 Comparison to literature

Finally, the heat transfer coefficients — are determined for the simulation and experimental results (region without any bubble formation only) and are compared to a literature correlation for the case 'Heat Emission at Lower Surface (Upper Surface Cooled)' suggested by Kast and Klan [7] in Figure 11.

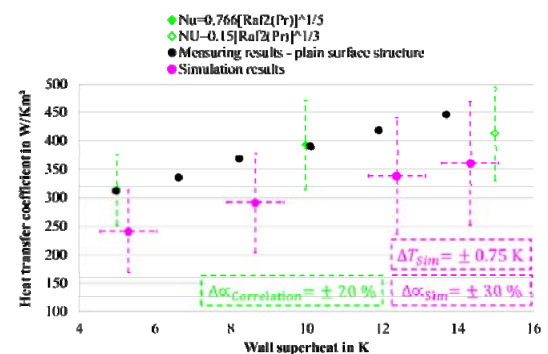


Figure 11. Heat transfer coefficient  $\alpha$  versus wall superheat – comparison of measuring and simulation results to literature.

According to this, the Nusselt-number is determined for laminar flows via

— and for turbulent flows

$$\text{Nu} = 0.15[\text{Raf}_2(\text{Pr})]^{1/3} \quad \text{with} \quad f_2(\text{Pr}) = \left[1 + \left(\frac{0.322}{\text{Pr}}\right)^{11/20}\right]^{-20/11}$$
 while fluid properties are used for the corresponding reference temperature. In figure 11 the results are opposed to each other. Here, the suggested uncertainty by Gorenflo and Kenning [1] for pool boiling correlations  $\Delta\alpha_{\text{Correlation}}$  as well as error bars to estimate the deviations between simulation and experimental result is further included.

As one can observe, the experimental results show a very good agreement to the laminar flow correlation while deviations occur at higher wall superheats for the turbulent flow correlation. In contrast to this, simulation results are approx. 30 % smaller and the wall superheat is predicted higher – up to 0.75 K. Even though there is a very good agreement between the experimental data and the correlations the differences between the measured values and the simulation results are addressed to the fact that the heat input of the heat flux sensor has been applied without taking the radial heat losses into account. The actual heat flux arriving on top of the surface is expected to be smaller. Moreover, its influence on the difference in wall superheat has not been taken into account. For this reason the need of adapting the experimental data seems to be necessary and will be investigated by further simulations.

## 5. Conclusion

A reasonable COMSOL model has been developed in order to estimate heat losses and gains for predicting the boiling curve of a specific measuring set-up. Thus, simulation results have been obtained that overestimate measuring results of a plain surface structure (temperature measurement inside the sample) at laminar flows only slightly, i.e. up to + 1 K. A rough sensitivity analysis could show that the isobaric thermal expansion coefficient  $\beta$  seems to be the most appropriate parameter in order to fit the model even more to the experimental data. In contrast to this, there is no recognizable influence to the sample temperature neither by decreasing the heat input from the heater stump to the sample insulation nor by increasing the heat losses to the environment or through increasing the thermal conductivity inside the low pressure steam chamber.

Predicting the boiling curve for the plain surface structure considerable deviations for the heat flux and the wall superheat have to be taken into account. Thus, a reduction in heat flux of 20 % and an increase in wall superheat of approx. 1 K could have been observed showing the necessity for rectifying the measuring data. Contrary to this, the influence of heat losses and gains seems to be negligible creating the boiling curve for the metallic short fiber structure. Here, a decrease of the actual heat flux arriving on top of the surface of approx. 2 % was found while the wall temperature increases with a value of 0.03 K only very slightly. Nevertheless, it is further necessary to prove how the turbulent fluid flow in the upper part of the pool influences the heat transfer alongside the sample insulation and therefore the radial heat losses or the actual heat flux arriving on top of the surface respectively.

Comparing the heat transfer coefficients of the plain surface structure both for the measuring and simulation results to literature correlations could show a very good agreement between the experimental data and the correlations. The simulation results were approx. 30 % lower while the suggested uncertainties of the correlations are  $\pm 20\%$  and close to this values. Nevertheless, the need of adapting the experimental data could have been observed and will be the focus of further investigations.

## 6. Acknowledgements

This work was funded by the German Federal Ministry of Industry and Technology (BMWi) with the project “SORCOOL”, grant no. 0327423B. The funding program is executed by the Project Management Organisation Jülich (PTJ).

## 7. References

- [1] Gorenflo, D., Kenning, D., VDI Heat Atlas – ‘H2 Pool Boiling’, page 757-792, Springer-Verlag, Berlin Heidelberg (2010)
- [2] Stephan, P., VDI Heat Atlas – ‘H Boiling’, page 753-756, Springer-Verlag, Berlin Heidelberg (2010)
- [3] Stephan, P., VDI Heat Atlas – ‘B1 Fundamentals of Heat Transfer’, page 17-29, Springer-Verlag, Berlin Heidelberg (2010)

[4] Wagner, W. Kretzschmar, H. J., International Steam Tables - Properties of Water and Steam based on the Industrial Formulation IAPWS-IF97, Springer-Verlag, Berlin, 2nd edition, 2008

[5] Schnabel, L. Scherr, Ch. Weber, C., Water as Refrigerant – experimental evaluation of boiling characteristics at low temperatures and pressures, International Sorption Heat Pump Conference 2008, 23-26 September, Seoul (Korea)

[6] COMSOL Model Gallery, Buoyancy Flow in Free Fluids, Model ID: 665, available at <http://www.comsol.com/showroom/gallery/665/>

[7] Kast, W., Klan, H., (Thess, A.), ‘F2 Heat Transfer by Free Convection: External Flows’, page 667-673, Springer-Verlag, Berlin Heidelberg (2010)

[8] Thess, A., VDI Heat Atlas – ‘F3 Heat Transfer by Free Convection: Internal Flows’, page 673-680, Springer-Verlag, Berlin Heidelberg (2010)

[9] Herwig, H., Wärmeübertragung A-Z, Systematische und ausführliche Erläuterungen wichtiger Größen und Konzepte, Springer, 2000 (VDI-Buch)

[10] Kabelac, S., Vortmeyer, D., VDI Heat Atlas – ‘K1 Radiation of Surfaces’, page 948-960, Springer-Verlag, Berlin Heidelberg (2010)

[11] Stephan, P., Schaber, K., Stephan, K. Mayinger, F., Thermodynamik, Grundlagen und technische Anwendungen Band 1: Einstoffsysteme, 18. Auflage, Springer-Verlag, Berlin Heidelberg (2009)

## 8. Appendix

**Table 2:** Nomenclature

Quantity	Symbol of the quantity	Symbol of the unit
Acceleration of gravity	g	m/s <sup>2</sup>
Characteristic length	L	m
Coefficient of thermal expansion	$\beta$	1/K
Nabla operator	$\nabla$	-
Density	$\rho$	kg/m <sup>3</sup>
Diameter (outer)	D	m
Diameter (inner)	d	m
Difference operator	$\Delta$	-
Dynamic viscosity	$\eta$	Pa s
Emissivity	$\varepsilon$	-
Extended measuring uncertainty	k	-
Heat flow	$\dot{Q}$	W
Heat flux	$\dot{q}$	W/m <sup>2</sup>
Overall Heat transfer coefficient	$\alpha$	W/m <sup>2</sup> K
Height	h	m
Kinematic viscosity	$\nu$	m <sup>2</sup> /s
Length (T <sub>Sample</sub> - T <sub>Wat</sub> )	s	m
Nusselt number	Nu	-
Prandtl number	Pr	-
Radiation coefficient	C	W/m <sup>2</sup> K <sup>4</sup>
Rayleigh number	Ra	-
Specific heat capacity	c	J/kgK
Velocity field	u	m/s <sup>2</sup>
Stefan-Boltzmann's constant	$\sigma$	W/m <sup>2</sup> K <sup>4</sup>
Surface	A	m <sup>2</sup>
Thermal conductivity	$\lambda$	W/mK
Thermal diffusivity	$\kappa$	m <sup>2</sup> /s
Thermodynamic temperature	T	K
Celsius temperature	$\vartheta$	°C
Total pressure	p	Pa; bar
Grashof number	Gr	-

Subscripts and Abbreviations	Description
Act	Actual
0	Initial value
CC	Equivalent for convection and conduction
CCR	Equivalent for radiation, convection and conduction
Crit	Critical
Cu	Copper cylinder
Cyl	Cylinder
H	Heater
HF	Heat flux
HFS	Heat flux sensor
In	Input
In,radiation-conduction	Input of heat through radiation and conduction
m	Average
Max	Maximal value
MV	Measured value
p	Pressure
PMMA	Polymethylmethacrylate
PP	Polypropylene
R	Equivalent for radiation
Sat	Saturation
SA	Sensitivity analysis
Sim	Simulation
TFI	Turbulent Flow Interface
WSH	Wall super heat
1	Temperature of the heater boundary
2	Temperature of the colder boundary
*	Reference temperature